

## NUMERICAL SIMULATION OF TURBULENT PLUMES IN A CHANNEL FLOW: SETTLING VELOCITY AND TILTED-BOTTOM RAMP EFFECTS

L. C. Pinto<sup>a</sup>, L. F. R. Espath<sup>a</sup>, S Laizet<sup>b</sup> and J. H. Silvestrini<sup>a</sup>

<sup>a</sup>*Faculdade de Engenharia, Pontifícia Universidade Católica do Rio Grande do Sul, Av. Ipiranga 6681, 90619-900 Porto Alegre - RS, Brasil, leandrocomp@gmail.com, <http://www.pucrs.br/feng>*

<sup>b</sup>*Turbulence, Mixing and Flow Control Group, Department of Aeronautics, Imperial College London, London, SW7 2BY, United Kingdom*

**Keywords:** Turbulent plumes, Immersed Boundary Method, Particle Transport.

**Abstract.** In the present work, we investigate numerically by means of Direct Numerical Simulation (DNS) the mixing of fresh and salty water in a channel flow configuration along with particle settling processes. In particular, we focus on the influence of the settling velocity in the formation of the fingering instability and the effect of the slope in a bottom tilted ramp. Three-dimensional simulations were done for two settling velocity values while for two-dimensional simulations a slightly tilted ramp inside the computational domain was imposed for 4 different bottom slopes. This ramp is modelled using an Immersed Boundary Method (IBM) in order to mimic submarine configurations. We describe and illustrate the underlying physics of the particle settling processes under the influence of the fresh/salt water mixing layer. We present results without and with various slightly tilted ramps for different Richardson numbers and settling velocities for Reynolds number  $Re = 1500$ . The spatial flow structures of the longitudinal vortex formation in the mixing layer turbulence transition as well as the fingering instability caused by the settling particles at early stages of sedimentation process are investigated.

## 1 INTRODUCTION

Particle transport from turbid rivers to ocean continental shelves are systems of great importance in the formation of the submarine failures as slopes, canyons and delta fronts. The salt ocean water is normally heavier than fresh water with particles which causes the formation of a flow configuration called river plumes. Such river plumes can be transported over long horizontal distances on the combined buoyancy and the inertial effects. Those positive buoyant flows are known as hypopycnal turbulent flows (turbulent plumes).

Accordingly Lamb et al. (2010), when certain conditions of inertial effects, particle concentration, settling velocity and water depth are reached, the sediments starts to falling forming a descendent flow configuration called hyperpycnal plumes. There is a region along the river length called depth limited plume zone where a transition from the turbulent plume to a turbid current flow occurs. This transition causes the plunge of the particles which is associated with the effects of the depth water and the inlet flood discharge.

Numerical simulations for confined channel and open basin in laboratory scale configuration were earlier done by Henniger and Kleiser (2010), Henniger et al. (2010) and Henniger and Kleiser (2012). In such works the authors presented results of fresh/salt water interactions varying parameters as Reynolds number, Richardson number and settling particle velocity.

In this paper, we present two- and three-dimensional numerical simulations of turbulent plumes under the effect of two mean parameters, the settling velocity and the slope bottom tilted ramp. The main propose here is to analyse the flow physical changes which causes the instabilities and the suspended and deposit of particles along the channel bottom.

The paper are organized as follows: In the section 2 the governing equations are introduced where the numerical methodology is described including the main initial and boundary conditions used in the problem. The analyses of the results are presented in the section 3 for three main configurations. First simulations for only salinity mixing layer, second the introduction of particle concentration and finally the results for the tilted ramp case. At the final section we present the main conclusions and recommendations of the work.

## 2 GOVERNING EQUATIONS AND NUMERICAL METHODOLOGY

To numerically compute turbulent plumes we need to solve the following governing equations (Henniger and Kleiser (2012)),

$$\frac{\partial u_j}{\partial x_j} = 0, \quad (1a)$$

$$\frac{\partial u_i}{\partial t} + u_j \frac{\partial u_i}{\partial x_j} = -\frac{\partial p}{\partial x_i} + \frac{1}{Re} \frac{\partial^2 u_i}{\partial x_j \partial x_j} + e_i^g (Ri_p c_p + Ri_s c_s) + f_i, \quad (1b)$$

$$\frac{\partial c_s}{\partial t} + u_j \frac{\partial c_s}{\partial x_j} = \frac{1}{Re S c_s} \frac{\partial^2 c_s}{\partial x_j \partial x_j} + f_{c_s}, \quad (1c)$$

$$\frac{\partial c_p}{\partial t} + (u_j + u_s e_j^g) \frac{\partial c_p}{\partial x_j} = \frac{1}{Re S c_p} \frac{\partial^2 c_p}{\partial x_j \partial x_j} + f_{c_p}. \quad (1d)$$

In these equations  $u_i$  and  $p$  are the velocity and pressure fields respectively,  $c_s, c_p$  are the salinity and particle concentration,  $u_s$  the Stokes settling velocity,  $e_j^g = (0, -1, 0)$  is the unit vector acting in the gravity acceleration direction,  $f_i$  is an external force, and  $f_{c_s}, f_{c_p}$  are source terms for the salinity and particle transport equations respectively.

The non-dimensional parameters of the flow are: the Reynolds number  $Re = \tilde{U} \tilde{h} / \tilde{\nu}$ , the Richardson numbers  $Ri_p = \tilde{g}_p^r \tilde{h} / \tilde{U}^2$ ,  $Ri_s = \tilde{g}_s^r \tilde{h} / \tilde{U}^2$  for particle and salinity concentrations

respectively and the Schmidt numbers  $Sc_p = \tilde{\nu}/\tilde{D}_p, Sc_s = \tilde{\nu}/\tilde{D}_s$  associated to the diffusion of the particle and salinity concentrations ( $\tilde{\cdot}$  indicates dimensional quantities). In these non-dimensional parameters  $\tilde{U}$  is the inflow bulk velocity,  $\tilde{h}$  the inflow depth,  $\tilde{g}_i^r$  the reduced gravitational acceleration;  $\tilde{D}_i$  the diffusivity coefficient and  $\tilde{\nu}$  the kinematic viscosity.

The above governing equations are numerically solved using the in-house numerical code `incompact3d`. The spatial discretization of these equations is done through a compact finite difference scheme of sixth order (Lele, 1992), and the time advancement is determined by a third order Adams-Bashforth scheme. More detail about the numerical schemes used here can be found in Laizet and Lamballais (2009); Laizet and Li (2011).

A new set of boundary conditions need to be consider in order to implement a ramp at the bottom channel. That means a no-slip boundary condition for the velocity field  $u_i$ , a deposit condition for the particle concentration  $c_p$  and a no-flux condition for the salinity  $c_s$  need to be respected over the sloped surface ramp. For this task we use the Immersed Boundary Method (IBM), which introduces the extra force  $f_i$  and the source terms  $f_{c_s}, f_{c_p}$  to imposed the boundary conditions as shown below.

Considering the time advancing temporal scheme of Adams-Bashforth method, the forcing term  $f_i$  in the equation (1b) is defined by:

$$c_k f_i^{k+1} = \varepsilon(-a_k G_i^k - b_k G_i^{k-1} + c_k \frac{\partial p^k}{\partial x_i} + \frac{u_{i_0}^{k+1} - u_i^k}{\Delta t}), \quad (2)$$

where the Adams-Bashforth coefficients are  $a_k = 3/2, b_k = -1/2$  and  $c_k = a_k + b_k$ . the  $k = t_k/\Delta t$  index correspond to the considered time  $t_k$ .  $G_i$  represents the convective-diffusive-gravitational term, which is given by:

$$G_i = -u_j \frac{\partial u_i}{\partial x_j} + \frac{1}{Re} \frac{\partial^2 u_i}{\partial x_j \partial x_j} + e_i^g (Ri_p c_p + Ri_s c_s). \quad (3)$$

The imposition of  $u_{i_0}^{k+1}$  in the equation (2) must satisfy the no-slip condition in the ramp surface.  $\varepsilon$  is responsible for identifying which mesh points are in the inner ( $\varepsilon = 1$ ) or outer ( $\varepsilon = 0$ ) region of the ramp. Let  $y_r(x_1)$  the function representing the ramp (Figure 1), we impose  $u_{i_0} = 0$  for  $x_2 \leq y_r(x_1)$ .

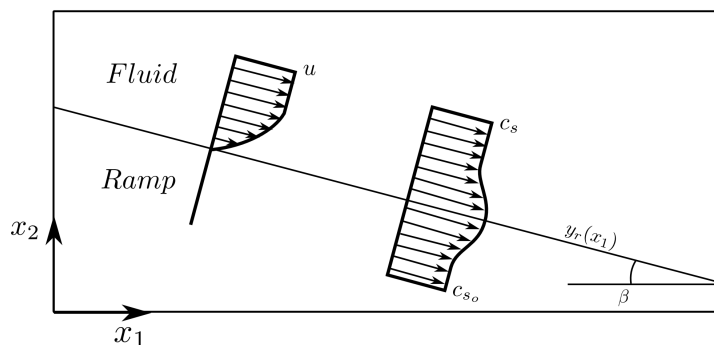


Figure 1: Representation of no-slip velocity and no-flux salinity conditions at the ramp.

For the salinity, the no-flux boundary condition need to be imposed at the boundary of the ramp surface. To satisfy this condition the same IBM method is used where the  $f_{c_s}$  term in the

equation (1c) is computed as:

$$c_k f_{c_s}^{k+1} = \varepsilon(-a_k H^k - b_k H^{k-1} + \frac{c_{s_0}^{k+1} - c_s^k}{\Delta t}). \quad (4)$$

The  $H$  term corresponds to the convective-diffusive terms in the transport equation (1c), being expressed by:

$$H = -u_j \frac{\partial c_s}{\partial x_j} + \frac{1}{ReSc_s} \frac{\partial^2 c_s}{\partial x_j \partial x_j}. \quad (5)$$

The value of  $c_{s_0}^{k+1}$  is obtained by reflecting the salinity field  $c_s$  from the upside of the ramp to the downside as is shown in figure (1). This process allow us to recover the no-flux salinity boundary condition at the ramp.

Finally, for the particle concentration  $c_p$  a deposit condition is imposed where  $f_{c_p}$  in equation (1d) is computed as:

$$c_k f_{c_p}^{k+1} = \varepsilon(-a_k I^k - b_k I^{k-1} + \frac{c_{p_0}^{k+1} - c_p^k}{\Delta t}), \quad (6)$$

where  $I$  represents the convective-diffusive terms of the transport equation (1d), and it is expressed as:

$$I = -(u_j + u_s e_j^g) \frac{\partial c_p}{\partial x_j} + \frac{1}{ReSc_p} \frac{\partial^2 c_p}{\partial x_j \partial x_j}. \quad (7)$$

In order to compute  $c_{p_0}^{k+1}$  an convection equation is used:

$$\frac{\partial c_{p_0}}{\partial t} - u_p^s \frac{\partial c_{p_0}}{\partial x_2} = 0. \quad (8)$$

With this condition the particles deposited at the bottom of the ramp cannot move by gravitational effect.

## 2.1 Boundary conditions

The inflow boundary conditions ( $x_1=0$ ) are prescribed using,

$$c_p = F \quad (9a)$$

$$c_s = 1 - F \quad (9b)$$

$$u_i = (F, 0, 0) \quad (9c)$$

with

$$F(x_2) = \frac{1}{2} \left[ 1 + \operatorname{erf} \left\{ \frac{\sqrt{\pi}}{\delta h} (x_2 - x_2^{if}) \right\} \right] \quad (10)$$

The parameter  $x_2^{if}(t)$  indicate the vertical position of the velocity and concentration interfaces while  $\delta h$  is the concentration profile and shear layer thickness. This shear layer is excited by an vertical movement of the interface position imposed by  $x_2^{if}(t) = x_2^{if,avg} + x_2^{if,rand}(t)$ . In this equation  $x_2^{if,avg}$  is the mean value (fixed) while  $x_2^{if,rand}(t)$  is the fluctuation imposed. This perturbation will ensure a fast transition of the mixing layer.

The outflow boundary conditions ( $x_1=L_1$ ) are imposed as:

$$\frac{\partial c_p}{\partial t} + U^{b,1} \frac{\partial c_p}{\partial x_1} = 0 \quad (11a)$$

$$\frac{\partial c_s}{\partial t} + U^{b,1} \frac{\partial c_s}{\partial x_1} = 0 \quad (11b)$$

$$\frac{\partial u_i}{\partial t} + U_j^{b,u} \frac{\partial u_i}{\partial x_j} = 0 \quad (11c)$$

where  $U^{b,1}$  is the convection velocity in the normal direction of the outflow contour for the salinity and particle concentration fields, while  $U_j^{b,u}$  is the convection velocity of the vortices transported to the outside of the computational domain. In all simulation it was considered  $U^{b,1} = U_j^{b,u} = 1$ .

It was assumed here that the free surface at the top boundary ( $x_2=L_2$ ) are not deformed. This condition is satisfied when the no-flux of particle and salinity while free-slip for velocity fields are prescribed,

$$\frac{\partial c_p}{\partial x_2} = 0, \quad (12a)$$

$$\frac{\partial c_s}{\partial x_2} = 0, \quad (12b)$$

$$\left( \frac{\partial u_1}{\partial x_2}, u_2, \frac{\partial u_3}{\partial x_2} \right) = (0, 0, 0). \quad (12c)$$

Dirichlet no-slip are prescribed in the velocity components, convection for particle concentration and Newmann (no-flux) for salinity field are imposed in the bottom contours,

$$\frac{\partial c_p}{\partial t} - u_s \frac{\partial c_p}{\partial x_2} = 0 \quad (13a)$$

$$\frac{\partial c_s}{\partial x_2} = 0 \quad (13b)$$

$$u_i = 0 \quad (13c)$$

In the three-dimensional simulations it was used the free-slip boundary conditions for  $u_i$  while no-flux boundary conditions for  $c_p$  and  $c_s$  in direction  $x_3$ . All boundary conditions are represented in figure (2).

### 3 RESULTS AND DISCUSSIONS

#### 3.1 Salinity mixing layer

The main physical phenomena observed in stratified mixing layers is the Kelvin-Helmholtz (*K-H*) instability. The purpose of the first simulations presented here is to verify the influence of the inflow perturbation in a salinity mixing layer without particle concentration and ramp at the bottom. In this case we used a harmonic function applied in the inflow profile of velocity (equation 10), which is given by:

$$x_2^{if}(t) = x_o + A \sin(\omega t) \quad (14)$$

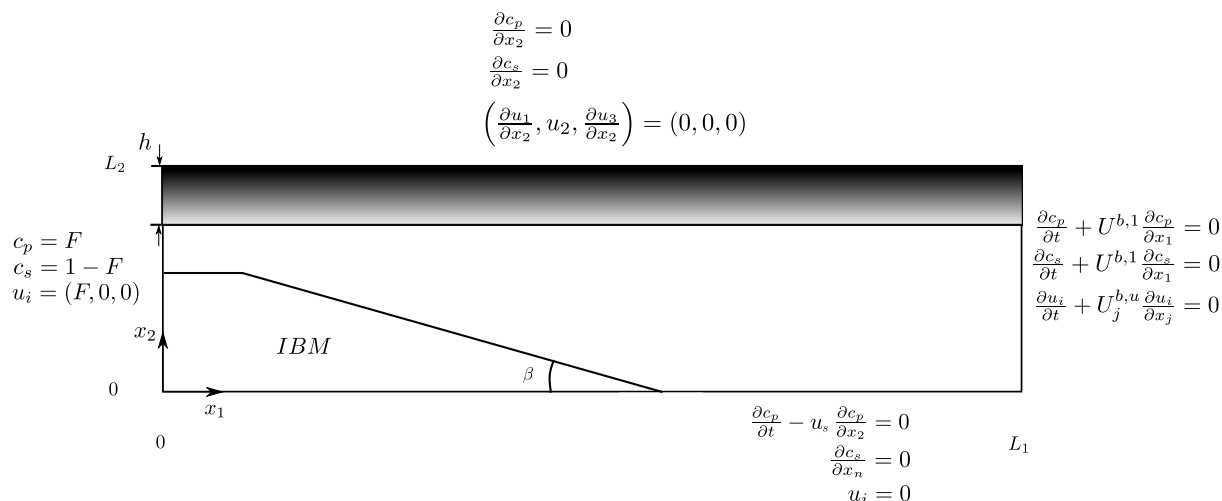


Figure 2: Sketch of the boundary conditions for channel ramp configuration.

It was considered the frequencies  $w = 0.5, 1.0, 1.5, 2.0$  e  $2.5$ , a vertical position  $x_o=3.0$  and a little noise perturbation was kept constant at  $A = 0.0005h$ . The computational parameters of this cases are: computational domain  $L_1, L_2 = 40, 4$ ; uniform mesh resolution  $n_1, n_2 = 1537, 193$ ;  $Re = 1500$ ;  $Ri_s = 0.5$  and  $Sc_s = 1$ .

It was observed in the figure 3 that the excitation frequency  $w$  causes a important influence in the  $K-H$  instability evolution. When the frequency decreases we observe the increasing of:

- the distance of the beginning instability relate to the inflow contour;
- the distance between the adjacent pair of vortices;
- the thickness of the unstable layer;
- the distance of the dissipation point of the instabilities relate to the inflow contour.

Quite similar results were obtained by [Henniger and Kleiser \(2010\)](#).

### 3.2 Particle-salt mixing layer

If only salinity was imposed to the flow, the inflow Richardson number ( $Ri_{in}$ ) correspond to the salinity Richardson number  $Ri_s$ . It means that the freshwater inflow is less denser than ambient salt fluid and the inflow becomes positively buoyant or hypopycnal. When the particle concentration was introduced the  $Ri_{in}$  changes depending of the volume fraction and the density of the particles. Accord to [Henniger et al. \(2010\)](#) the inflow Richardson number can be approximated by  $Ri_{in} \approx Ri_s - Ri_p$ . For this definition the inflow is hypopycnal if  $Ri_{in}$  is positive and hyperpycnal if it is negative.

Three-dimensional simulations for the case of hypopycnal inflow ( $Ri_{in} > 0$ , with introduction of particle mixing layer) were done using the following parameters:  $L_1, L_2, L_3 = 60, 4, 4$ ;  $n_1, n_2, n_3 = 2305, 193, 193$ ;  $Ri_p = 0.05$ ;  $Ri_s = 0.5$ . The Reynolds number was kept constant  $Re = 1500$  and the settling velocity was varied in  $u_s = 0.01$  and  $0.02$ . We run the simulations up to a dimensionless final time of  $t = 1400$ . As initial condition the equation 10 was imposed in all domain so that the initial suspended particle is  $m_{p0} = 60h \times 4h \times 1h \times c_p = 240c_p$

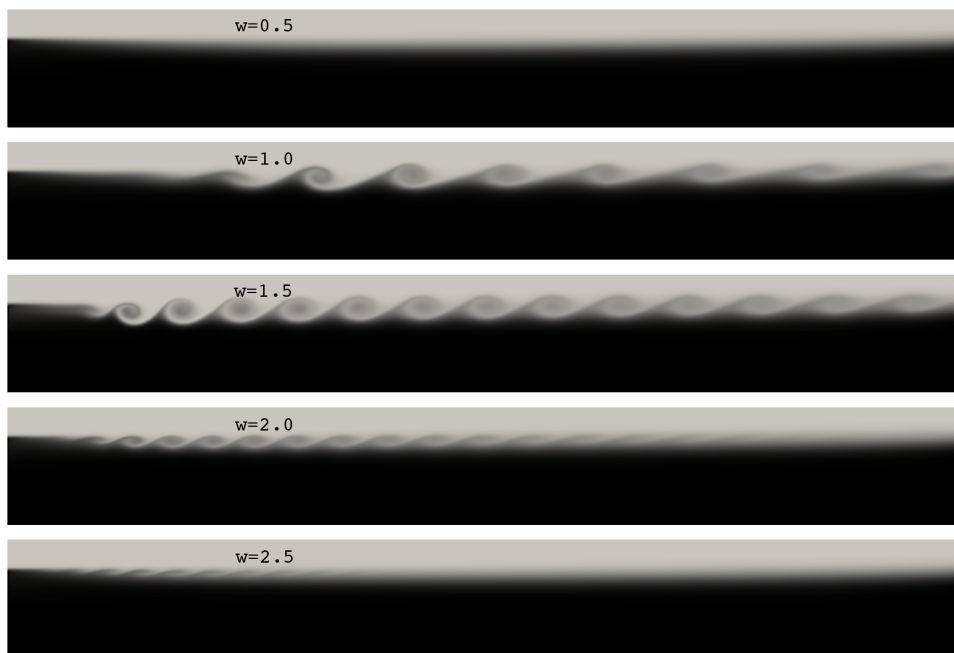


Figure 3: Salinity and particle concentration fields for different excitation frequencies.

Informations about the time variation of the particle concentration could be obtained by computing such global variables as the suspended particles ( $m_p$ ) and the sedimentation rate ( $\dot{m}_s$ ). These parameters were obtained respectively by:

$$m_p(t) = Ri_p \int_{\Omega} c \, d\Omega \quad (15)$$

where  $\Omega$  correspond to the computational domain, and,

$$\dot{m}_s(t) = \frac{1}{L_3} \int_0^{L_1} \int_0^{L_3} c_p(x_1, x_3, 0, t) u_s \, dx_3 dx_1. \quad (16)$$

The time variation of  $m_p$  and  $\dot{m}_s$  are presented in the figure 4. It is possible to verify the stabilization of the flow when the suspended material reaches the value  $m_p \approx 30$  for the case  $u_s = 0.02$  while in simulation with  $u_s = 0.01$ , the value of  $m_p$  increases during all simulation up to  $m_p \approx 40$ . Besides different initial conditions used here the final  $m_p$  results for  $u_s = 0.02$  is closer to the [Henniger et al. \(2010\)](#) numerical results.

When observed the time variation of  $\dot{m}_s$  in figure 4 (left) it is possible to identify the exact moment that the first particles are deposited. The simulation with  $u_s = 0.01$  presented lower values of  $\dot{m}_s$  than  $u_s = 0.02$ . Such result indicate the influence of the settling velocity in the suspended and deposited material with conservation of particles.

In figure 5 the bottom view of the isosurface particle concentration ( $c_p = 0.25$ ) are presented for the 3D simulations at the beginning of the simulation ( $t = 100$  for the simulation with  $u_s = 0.02$  and  $t = 135$  for the simulation with  $u_s = 0.01$ ). The particles are settled and it causes the formation of an instability known as *Fingering*. This instability are dissipated when the particles reaches the bottom domain forming the first deposition layers.

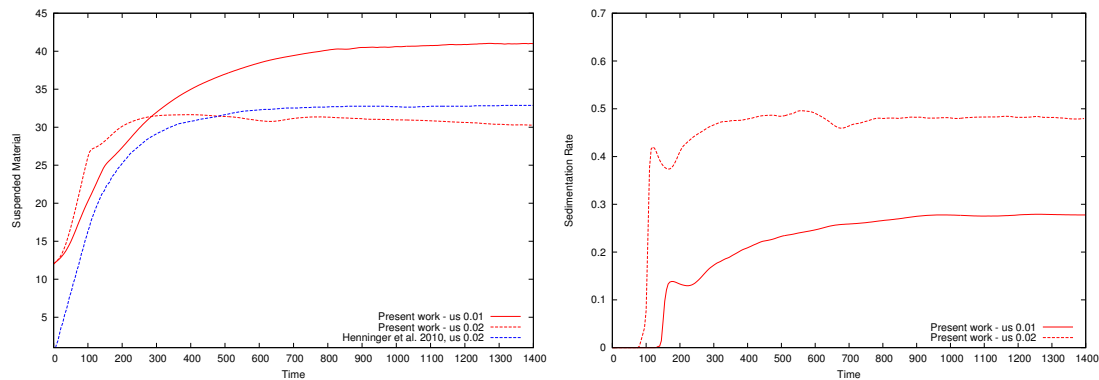


Figure 4: Time variation of suspended particle material ( $m_p$ , left) and sedimentation rate ( $\dot{m}_s$ , right) for the 3D simulations with  $u_s = 0.01; 0.02$ .

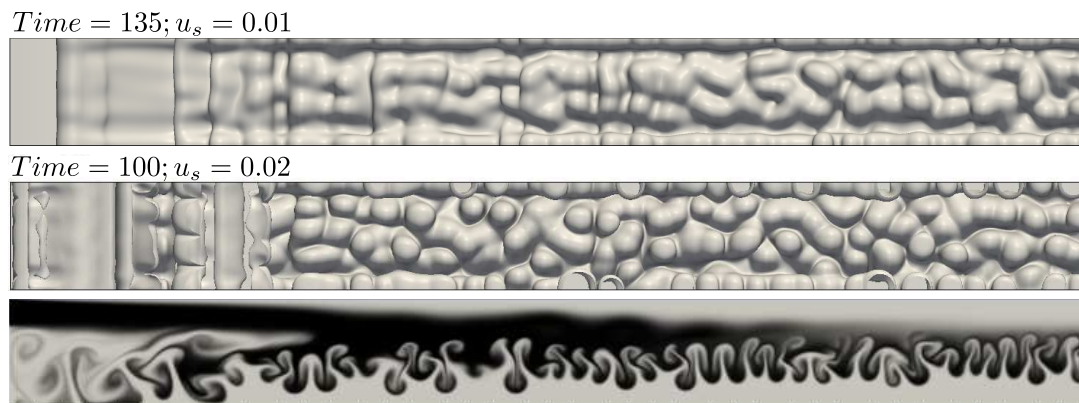


Figure 5: Fingering instability for simulations  $u_s = 0.01$  and  $u_s = 0.02$ .

After the dissipation of the *Fingering* the *K-H* instability appears, it turns turbulent up to the time  $t = 600$  and the flow reaches a visually stationary state around  $t = 800$ . In figure 6  $Q$ - criterion fields for  $t = 1000$  are presented for 3D simulations. It is possible to note a little reduction of the mixing layer thickness when the settling velocity is reduced from 0.02 to 0.01. In terms of flow size structures it is not possible to identify significant changes.

Three-dimensional views of the  $Q$ - criterion, the particle concentration and the salinity for simulation with  $u_s = 0.02$  are presented in figure 7. It can be observed the effect of the three-dimensional *K-H* vortices over the salinity and particle concentration fields.

### 3.3 Tilted ramp effect

In order to verify the effect of a tilted ramp at the bottom of the domain, more four two-dimensional simulations with different bottom slopes ( $S = \tan(\beta) = \infty, 0.2, 0.1, 0.05$ ) were done. The  $S = \infty$  correspond to the earlier no-ramp case. The domain configuration used was  $L_1, L_2 = 80, 4$ , with mesh resolution  $n_{x_1}, n_{x_2} = 3073, 193$ . Relate to the flow parameters the following values are imposed:  $Re = 1500, Ri_p = 0.05, Ri_s = 0.5, u_s = 0.02, Sc_p = Sc_s = 1$ . The ramp was located in the beginning of the domain at the position  $x_2 = 2.5h$  while the same earlier inflow conditions for velocity, particle and salinity are used.

The fields of the particle concentration ( $c_p$ ), the salinity ( $c_s$ ), and the vorticity ( $\omega_z$ ) for the final time  $t = 1000$  are presented respectively in the figure 8. It was observed a recirculation

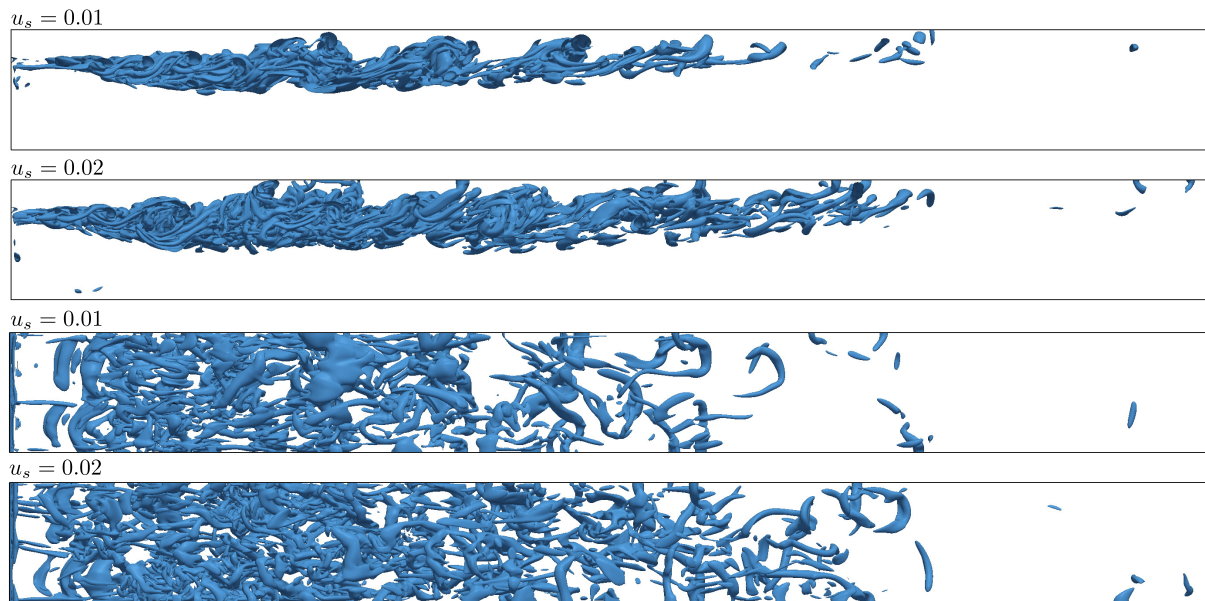


Figure 6: Three-dimensional fields of Q criteria  $Q = 0.10$  for simulations with  $u_s = 0.01$ ;  $0.02$  and  $t = 1000$ .

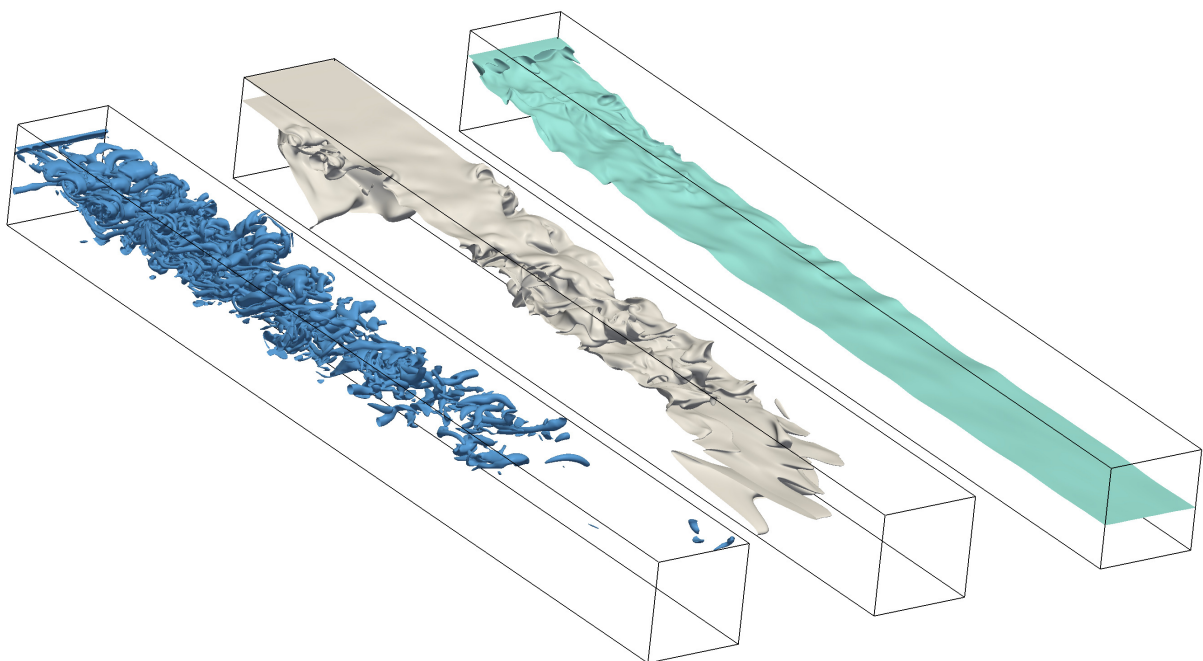


Figure 7: Three-dimensional fields of Q criteria  $Q = 0.10$  (left), particle concentration  $c_{part} = 0.95$  (center) and salinity  $c_s = 0.5$  (right) for simulation with  $u_s = 0.02$  and  $t = 1000$ .

in the inflow domain region for the case  $S = \infty$ . This recirculation was suppressed when the ramp was imposed in the other cases.

All simulations presented the formation of the  $K-H$  instability in the upper flow region (See the vorticity fields). The imposition of the ramp turns the flow confined, increasing its mean velocity which causes the pairing of the vortices in the mixing layer zone changing the vortex shedding frequency. This phenomena affect both distribution of suspended particles and the total deposition along the channel. It is possible to note also a wash effect in the salinity

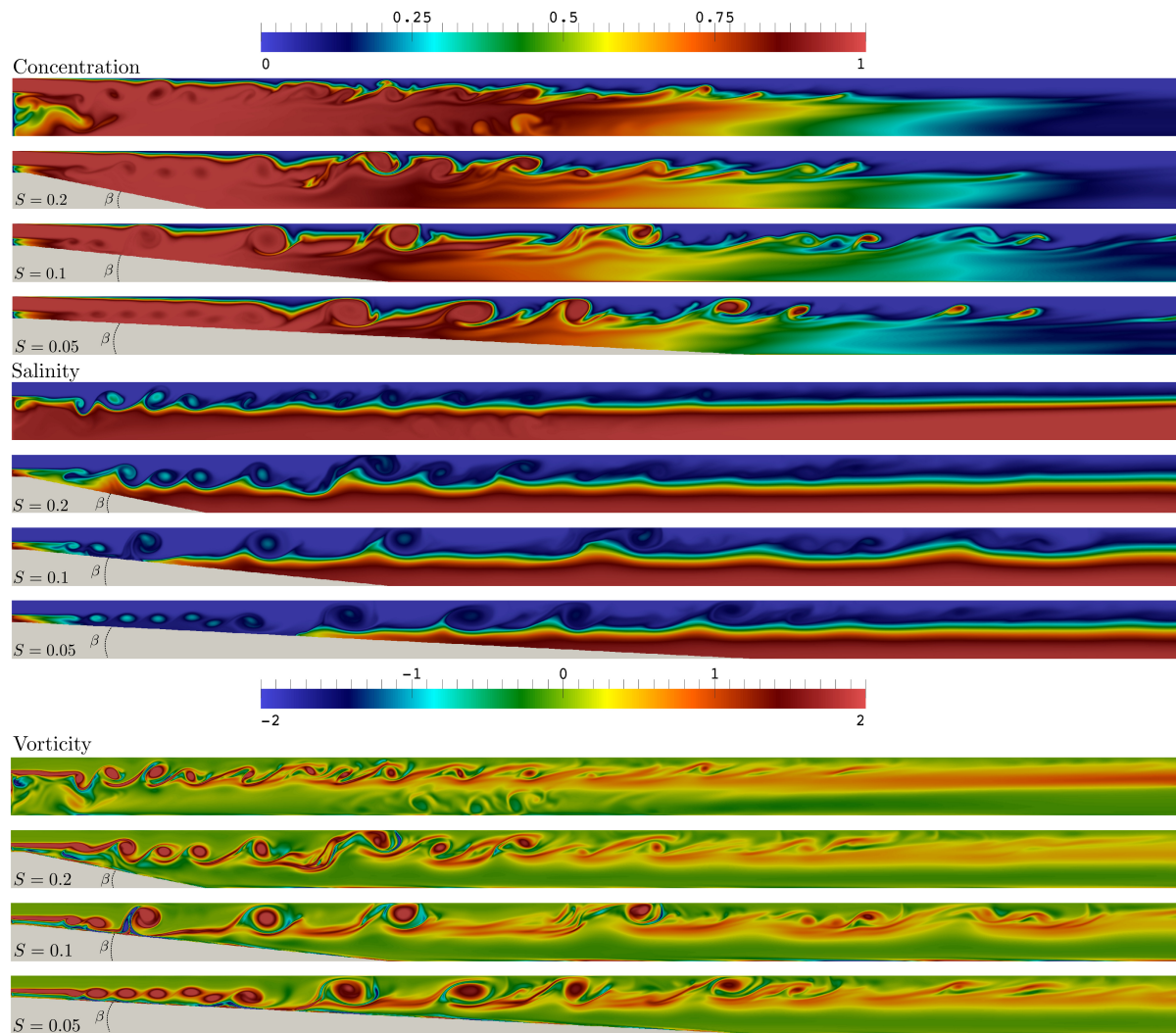


Figure 8: Fields comparison of particle concentration, salinity and vorticity for  $S = \infty, 0.2, 0.1, 0.05$ .

concentration for simulations with  $S = 0.05$ .

The time variation of the sedimentation rate for 2D ramp simulations are presented in figure 9. Comparing the results of the ramp simulations ( $S = 0.2, 0.1, 0.05$ ) with the no-ramp case ( $S = \infty$ ), it was noted a increasing of  $\dot{m}_s$  with  $S$ .

#### 4 CONCLUSIONS

In this paper first simulations for a flow plume in a channel are presented for two- and three-dimensional configurations. Qualitatively validating results are presented for a salinity mixing layer flow and it are in good agreement with numerical results by Henniger and Kleiser (2010).

In three-dimensional simulations for salinity and particle mixing layer it was observed the evolution of two main instabilities: *fingering* and *Kelvin-Helmholtz*. The *fingering* instability is observed in the initial phase of the simulation when the first particles reaches the bottom of the domain. Before the dissipation of the *fingering* processes, the flow starts its transition forming the *Kelvin-Helmholtz* vortices and at the final time of the simulation the mixing layer is completely turbulent. Our three-dimensional simulations shown that the mixing layer thickness

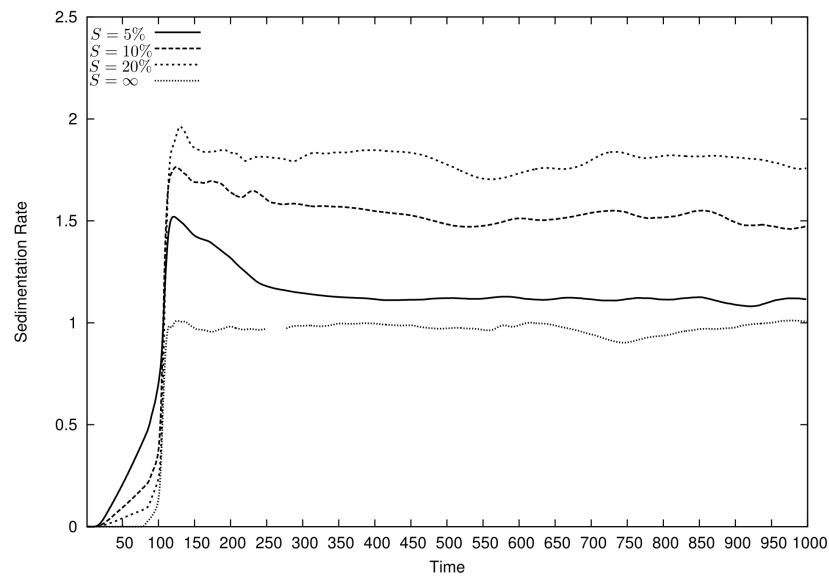


Figure 9: Time variation of deposit rate for ramp 2D simulations with  $S = \infty, 0.2, 0.1, 0.05$ .

increases with the settling velocity of the particle while little changes are observed in the flow structures.

In simulations with ramp configuration significant influence of the slope is observed in the shedding frequency of the *Kelvin-Helmholtz* vortices. The pairing of the vortices was affecting the distribution of suspended particles and the total deposition along the channel.

## 5 ACKNOWLEDGEMENTS

Present simulations have been carried out at the High Performance Computing facility of the Pontifical Catholic University of Rio Grande do Sul (LAD/PUCRS). The authors are grateful to Petrobras for supporting this research. JHS acknowledges financial assistance of CNPq.

## REFERENCES

- Laizet S. and Lamballais E. High-order compact schemes for incompressible flows: A simple and efficient method with quasi-spectral accuracy. *J. Comp. Phys.*, 228:5989–6015, 2009.
- Henniger R. and Kleiser L. Simulation of gravity-driven flows using an iterative high-order accurate Navier-Stokes solver. In *ERCOFTAC, Direct and Large-Eddy Simulation VII*, pages 121–127. Trieste, 2010.
- Henniger R. and Kleiser L. Temporal evolution, morphology, and settling of the sediment plume in a model estuary. *Phys. Fluids*, 24(086601):1–31, 2012.
- Henniger R., Kleiser L., and Meiburg E. Direct numerical simulations of particle transport in a model estuary. *J. Turbulence*, 11(39):1–31, 2010.
- Laizet S. and Li N. Incompact3d: A powerful tool to tackle turbulence problems with up to  $O(10^5)$  computational cores. *Int. J. Numer. Methods Fluids*, 67:1735–1757, 2011.
- Lamb M., McElroy B., Kopriva B., Shaw J., and Mohrig D. Linking river-flood dynamics to hyperpycnal-plume deposits: Experiments, theory and geological implications. 122:1389–1400, 2010.
- Lele S. Compact finite difference schemes with spectral-like resolution. *J. Comp. Phys.*, 103:16–42, 1992.